ChemComm

COMMUNICATION

View Article Online
View Journal

Check for updates

Cite this: DOI: 10.1039/d1cc01462e

Received 18th March 2021,
Accepted 9th April 2021

DOI: 10.1039/d1cc01462e

rsc.li/chemcomm

Published on 22 April 2021. Downloaded by BUTLER UNIVERSITY on 5/15/2021 12:34:12 PM.

A tumor-targeted near-infrared fluorescent probe for HNO and its application to the real-time monitoring of HNO release *in vivo*†

Ziyin Chai,[ab] Diankai Liu,[a] Xiaoyi Li,[a] Yanyan Zhao,[a] Wen Shi, *[ab] Xiaohua Li [a] and Huimin Ma *[ab]

Nitroxyl (HNO) is a promising regulator for cancer therapy. Here, we develop a tumor-targeted near-infrared fluorescent probe for HNO and utilize it in the real-time imaging of HNO release *in vivo*.

Starting with the seminal discovery of the gasotransmitter nitric oxide (NO), the field of reactive nitrogen species has been attracting expanding interest.[1] Generally, NO is produced in endothelial cells and is responsible for vasodilation. Pharmacological action of the well-known nitroglycerin can be ascribed to its capability of producing NO upon administration.[2] In past decades, the potential pharmacological effects of NO on cancer have been explored greatly, which has led to NO donors being seen as promising tumor cytotoxic agents.[3] Recently, nitroxyl (HNO), the one-electron reduced form of NO, has emerged as a new player with fascinating therapeutic potential since it exhibits orthogonal biological effect on NO.[4] For example, HNO treatment induces the death of non-small cell lung cancer cells and colon cancer cells.[5] In a subcutaneous xenograft model of pheochromocytoma, HNO donor, Angeli's salt (AS), markedly inhibited tumor growth.[6] However, compared to NO, HNO is much less understood. So far, the biological pathway by which HNO exerts its anticancer activity remains speculative and its relationship with NO is a matter of debate. These are largely due to the lack of a proper method for detecting HNO efficiently since the molecule is highly reactive toward thiols.[7] On the other hand, although various HNO donors for cancer therapy have been reported, evaluating their efficiency for generating HNO in tumors is still difficult.[8] Therefore, developing suitable fluorescent probes to image HNO *in vivo* is of great importance.

Toward this end, a variety of fluorescent probes for HNO have been reported.[9] One of the general HNO sensing strategies relies on the reduction of Cu^{2+} to Cu^{+} in a fluorescent metallochelate, which however suffers from severe interferences by other reductants such as ascorbate.[10] Alternatively, HNO-induced hydrolysis of a triarylphosphine caging group was proposed as a more selective method for HNO sensing.[11] Based on this reaction, several fluorescent probes for imaging HNO have been proposed.[12] Nevertheless, these probes mainly focused on capturing HNO in subcellular structures including endoplasmic reticulum and mitochondria (Table S1, ESI†),[13] and few of them aimed to study the effect of HNO in tumors, though it would be extremely helpful for evaluating HNO donors *in vivo*.

In this study, we report a new near-infrared (NIR) fluorescent probe (BHXP) for HNO with tumor-targeted ability *in vivo*. The probe was constructed with a hemicyanine NIR fluorophore (BHX, Scheme S1, ESI†), in which the triarylphosphine group was adopted to cage the fluorescence of BHX, and can be selectively cleaved by HNO to retrieve BHX's fluorescence (Scheme 1). Besides, biotin, which has been widely used for tumor-targeted delivery because of the overexpression of the biotin receptor (BR) in some cancer cells, was introduced to confer on the probe a targeting ability.[14] As a result, the probe was capable of imaging the intratumoral HNO release from AS *in vivo*.

The reactivity of BHXP with HNO donor, AS, was assessed firstly. As shown in Fig. 1, the probe exhibits a maximum absorption at 607 nm, and is nearly nonfluorescent ($\Phi < 0.01$) in PBS. Nevertheless, after reacting with 2 equivalents of AS, the

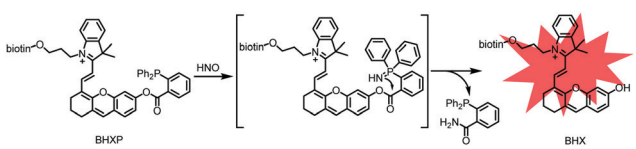

Scheme 1 The sensing mechanism of BHXP toward HNO.

[a] *Beijing National Laboratory for Molecular Sciences, Key Laboratory of Analytical Chemistry for Living Biosystems, Institute of Chemistry, Chinese Academy of Sciences, Beijing 100190, China. E-mail: shiwen@iccas.ac.cn, mahm@iccas.ac.cn*
[b] *University of Chinese Academy of Sciences, Beijing 100049, China*

† Electronic supplementary information (ESI) available. See DOI: 10.1039/d1cc01462e

Published on 22 April 2021. Downloaded by BUTLER UNIVERSITY on 5/15/2021 12:34:12 PM.

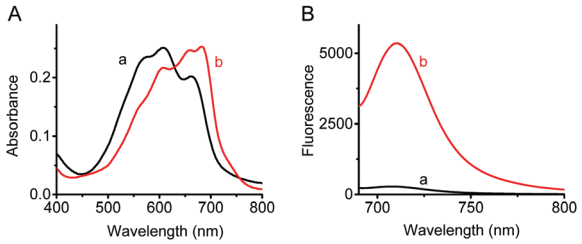

Fig. 1 (A) Absorption and (B) fluorescence spectra of BHXP (10 μM) without (a) and with (b) AS (20 μM) in PBS. λ_{ex} = 670 nm.

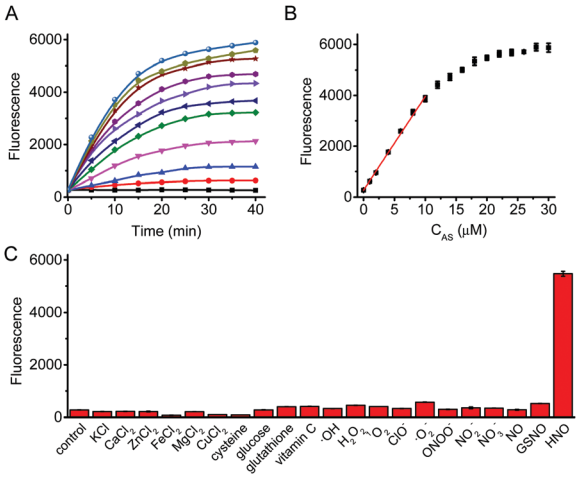

Fig. 2 (A) Kinetic curves of BHXP (10 μM) with different concentrations of AS (0, 1, 2, 5, 8, 10, 12, 15, 20, 25, and 30 μM). (B) A plot of the fluorescence intensity toward AS in the range of 0–30 μM. (C) The fluorescence responses of BHXP (10 μM) to various species: control; KCl (150 mM); $CaCl_2$ (1 mM); $ZnCl_2$ (100 μM); $FeCl_2$ (100 μM); $MgCl_2$ (1 mM); $CuCl_2$ (10 μM); cysteine (1 mM); glucose (10 mM); glutathione (1 mM); vitamin C (1 mM); •OH (100 μM); H_2O_2 (100 μM); $^1O_2$ (100 μM); ClO^- (100 μM); $•O_2^-$ (100 μM); $ONOO^-$ (100 μM); NO_2^- (100 μM); NO_3^- (100 μM); NO (100 μM); GSNO (100 μM); and HNO (*i.e.*, AS) (20 μM). $\lambda_{ex/em}$ = 670/708 nm.

reaction system displays a redshifted absorption at 682 nm, accompanied by about 20-fold fluorescence enhancement at 708 nm (Φ = 0.18, Fig. 1B). This phenomenon demonstrated that BHXP could serve as an NIR fluorescence off–on probe for detecting HNO in aqueous media. Additionally, HPLC and mass spectral analysis were conducted to verify the reaction mechanism. As shown in Fig. S10A (ESI†), BHX and BHXP display chromatographic peaks at 14.6 min and 21.0 min, respectively. After treating BHXP with AS for 30 min, there is a distinct product peak with retention time of 14.6 min and *m*/*z* 654.3 (Fig. S10C, ESI†). Additionally, an HNO scavenger (*N*-acetyl cysteine[12b]) can significantly inhibit the fluorescence of the reaction system (Fig. S10B, ESI†). These results indicated that HNO reacted with the ester bond of the recognition group, releasing the fluorophore BHX.

Then, the reaction conditions were investigated. The probe was relatively stable between pH 4 and pH 10, but displayed a large fluorescence increase after reaction with AS when the pH was above 6, suggesting its applicability at normal physiological pH (~7.4) and slightly acidic pH in cancerous tumor (Fig. S11A, ESI†). The reaction temperature varying from 25 °C to 40 °C has no obvious effect on the fluorescence (Fig. S11B, ESI†). Besides, the reaction kinetics of BHXP with different concentrations of AS was examined. The fluorescence of the reaction systems can nearly reach a plateau within 30 min, as shown in Fig. 2A. Thus, BHXP is quite suitable for biological applications.

Under the optimized conditions (reaction at 37 °C and pH 7.4 for 30 min), the fluorescence intensity (F) at 708 nm of the probe was found to be linear in the range of 0–10 μM AS (Fig. 2B), with an equation of $F = 368.8 \times c\,(AS) + 270.4$ (R = 0.997). The detection limit was determined to be 57 nM AS ($3\sigma/s$), indicating high sensitivity.

The selectivity of BHXP was evaluated. The tested potential interfering species in biological systems included inorganic salts, reductive species, and reactive oxygen species. As shown in Fig. 2C, these species show no significant response to the probe, with the exception of HNO. Especially, the effect of *S*-nitrosoglutathione (GSNO), which has been reported to interfere with HNO sensing in previous methods,[15] is negligible in the present system. The excellent selectivity of BHXP ensures its practical applications in cells and *in vivo*.

The toxicity of BHXP to various cells was evaluated by MTT assay. As shown in Fig S12 (ESI†), all the tested cell lines display >80% viability even when incubated with 20 μM BHXP for 24 h, suggesting good biocompatibility.

The applicability of BHXP for specific detection of HNO in living cells was then examined. Two cancer cell lines, HeLa and HepG2 with BR positive expression, and two normal cell lines, COS-7 and HK-2 with BR negative expression, were used.[16] These cells were incubated with BHXP in parallel for 30 min and washed with PBS. After the introduction of AS to each cell line, the fluorescence of HeLa and HepG2 cells increased significantly within 30 min, whereas that of COS-7 and HK-2 cells hardly increased (Fig. 3). This implies that the biotin subunit may promote probe accumulation in cancer cells (*i.e.*, BR-mediated endocytosis may play an important role in the entry of the probe into cells), thus generating considerable fluorescence. To further confirm this mechanism, HeLa and HepG2 cells were pre-saturated with 50 μM biotin for 30 min and then treated with BHXP and AS as above. In this case, the fluorescence enhancements were significantly inhibited, which can be attributed to the fact that the blocking of BR by biotin hindered BHXP from targeting the cells (Fig. S13, ESI†). These results indicate that BHXP can be used as a tumor-targeted probe for HNO imaging.

To study the tumor-targeting ability of the probe *in vivo*, mice with xenografted HeLa tumors were used as a model. First, the mice were intravenously administrated with BHX (the precursor of the probe) and imaged with *in vivo* imaging equipment (*in vivo* master). As shown in Fig. S14 (ESI†), after injection, BHX may distribute in the body, and mainly concentrates in the liver and kidney, which is a common way for metabolization. After 4 h, BHX displays a much stronger fluorescence in the tumor, suggesting that BHX with a biotin subunit can accumulate in this region efficiently. As a control, HXPI[17] with a similar hemicyanine skeleton but without the

 This journal is © The Royal Society of Chemistry 2021

Published on 22 April 2021. Downloaded by BUTLER UNIVERSITY on 5/15/2021 12:34:12 PM.

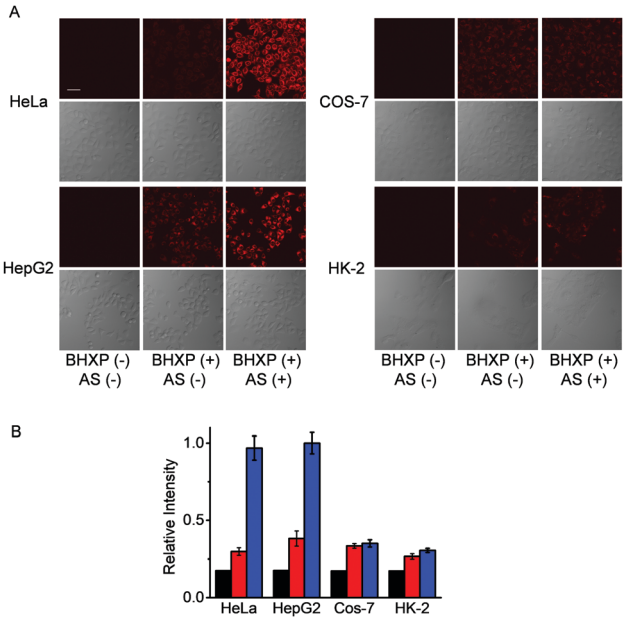

Fig. 3 (A) Fluorescence and differentiation interference contrast (DIC) images of different cell lines. (B) The relative intensities of the corresponding fluorescence images from panel (A); black bars: blank cells; red bars: cells incubated with BHXP (10 μM); blue bars: cells incubated with BHXP, washed, and then treated with AS (20 μM). Scale bar: 50 μm.

biotin subunit does not show any significant accumulation in the tumor region, and its fluorescence signal disappears quickly in the body. Moreover, as depicted in Fig. 4, after intravenous injection of BHXP for 4 h and then AS into the mice, real-time imaging results show that a significant NIR fluorescence gradually emerges in the tumor within 90 min (Fig. 4). In contrast, we cannot observe any obvious fluorescence in the tumor region in the control group injected with saline, though considerable fluorescence appears in the liver and kidney. All the above observations clearly indicate that the biotin subunit has a definite tumor-targeting function, and our probe can image HNO release in real time in tumors.

To further demonstrate that BHXP can react with HNO *in vivo*, additional experiments were performed by intratumoral injection. The probe was injected intratumorally into mice, and

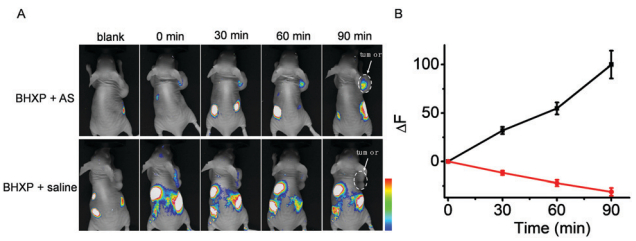

Fig. 4 (A) Representative *in vivo* fluorescence images of tumor-bearing mice (n = 3). The mice were intravenously administrated with BHXP (500 μM in 200 μL of saline). After 4 h, AS (1 mM in 200 μL of saline) or saline (control, 200 μL) was injected through the tail vein, and the mice were imaged at different time points. (B) Relative fluorescence changes in the tumor regions in the AS (black) and control (red) groups. ΔF is the fluorescence difference between a given time point and 0 min.

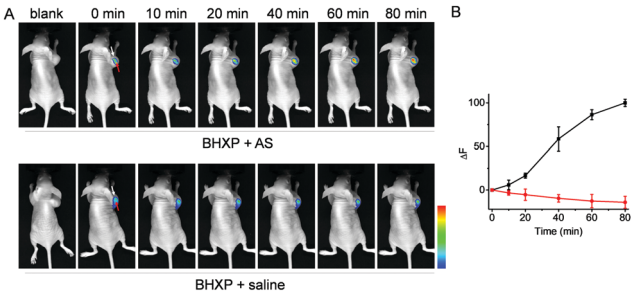

Fig. 5 (A) Representative *in vivo* fluorescence images of tumor-bearing mice (n = 3). The mice were intratumorally administrated (red arrow) with BHXP (200 μM in 100 μL of saline). After 30 min, AS (400 μM in 100 μL of saline) or a saline (control, 100 μL) was injected subcutaneously near the tumor (white arrow), and the mice were imaged at different time points. (B) Relative fluorescence changes in the tumor regions in the AS (black) and control (red) groups. ΔF is the fluorescence difference between a given time point and 0 min.

after 30 min AS was injected subcutaneously near to but outside of the tumor region (avoiding direct contact). In this case, there emerged a progressive fluorescence enhancement (Fig. 5). Meanwhile, in the control group, a saline injection did not lead to any fluorescence in the tumor. These results suggested that the BHXP probe can serve as a useful tool for evaluating the effect of HNO donors *in vivo*.

In summary, we have reported BHXP as a tumor-targeted NIR probe, which is composed of biotin as the tumor-targeted group and triarylphosphine as the HNO sensing group. The probe shows an NIR fluorescence off–on response toward HNO with high selectivity and sensitivity. Moreover, the probe displays excellent tumor-targeting abilities. These features mean the probe is capable of imaging HNO in cells and HNO release from its donors in tumors of mice *in vivo*. This probe may also be useful for assessing the potential therapeutic effects of HNO donors for cancer treatment.

This work is supported by grants from the NSF of China (no. 21922412, 21820102007, 21775152, and 22074151).

Conflicts of interest

There are no conflicts to declare.

Notes and references

1 (*a*) L. J. Ignarro, G. M. Buga, K. S. Wood, R. E. Byrns and G. Chaudhuri, *Proc. Natl. Acad. Sci. U. S. A.*, 1987, **84**, 9265–9269; (*b*) M. T. Ye, W. Hu, M. He, C. C. Li, S. Y. Zhai, Z. H. Liu, Y. Y. Wang, H. J. Zhang and C. Y. Li, *Chem. Commun.*, 2020, **56**, 6233–6236; (*c*) H. W. Liu, H. Y. Zhang, X. F. Lou, L. L. Teng, J. Yuan, L. Yuan, X. B. Zhang and W. H. Tan, *Chem. Commun.*, 2020, **56**, 8103–8106.
2 P. Pacher, J. S. Beckman and L. Liaudet, *Physiol. Rev.*, 2007, **87**, 315–424.
3 (*a*) C. X. Zhang and S. J. Lippard, *Curr. Opin. Chem. Biol.*, 2003, **7**, 481–489; (*b*) D. A. Wink, L. A. Ridnour, S. P. Hussain and C. C. Harris, *Nitric oxide*, 2008, **19**, 65–67.
4 W. Flores-Santana, D. J. Salmon, S. Donzelli, C. H. Switzer, D. Basudhar, L. Ridnour, R. Cheng, S. A. Glynn, N. Paolocci, J. M. Fukuto, K. M. Miranda and D. A. Wink, *Antioxid. Redox Signaling*, 2011, **14**, 1659–1674.

Published on 22 April 2021. Downloaded by BUTLER UNIVERSITY on 5/15/2021 12:34:12 PM.

5 (*a*) D. Basudhar, G. Bharadwaj, R. Y. Cheng, S. Jain, S. Shi, J. L. Heinecke, R. J. Holland, L. A. Ridnour, V. M. Caceres, R. C. Spadari-Bratfisch, N. Paolocci, C. A. Velazquez-Martínez, D. A. Wink and K. M. Miranda, *J. Med. Chem.*, 2013, **56**, 7804–7820; (*b*) A. Augustyniak, J. Skolimowski and A. Błaszczyk, *Chem. – Biol. Interact.*, 2013, **206**, 262–271.
6 D. A. Stoyanovsky, N. F. Schor, K. D. Nylander and G. Salama, *J. Med. Chem.*, 2004, **47**, 210–217.
7 (*a*) G. Keceli and J. P. Toscano, *Biochemistry*, 2014, **53**, 3689–3698; (*b*) E. H. S. Sousa, L. A. Ridnour, F. S. Gouveia, C. D. S. Silva, D. A. Wink, L. G. F. Lopes and P. J. Sadler, *ACS Chem. Biol.*, 2016, **11**, 2057–2065.
8 A. J. Norris, M. R. Sartippour, M. Lu, T. Park, J. Y. Rao, M. I. Jackson, J. M. Fukuto and M. N. Brooks, *Int. J. Cancer*, 2008, **122**, 1905–1910.
9 (*a*) R. Smulik-Izydorczyk, K. Dębowska, J. Pięta, R. Michalski, A. Marcinek and A. Sikora, *Free Radical Biol. Med.*, 2018, **128**, 69–83; (*b*) M. R. Cline and J. P. Toscano, *J. Phys. Org. Chem.*, 2011, **24**, 993–998.
10 A. T. Wrobel, T. C. Johnstone, A. D. Liang, S. J. Lippard and P. R. Fuentes, *J. Am. Chem. Soc.*, 2014, **136**, 4697–4705.
11 (*a*) J. A. Reisz, E. B. Klorig, M. W. Wright and S. B. King, *Org. Lett.*, 2009, **11**, 2719–2721; (*b*) J. A. Reisz, C. N. Zink and S. B. King, *J. Am. Chem. Soc.*, 2011, **133**, 11675–11685.
12 (*a*) J. B. Li, Q. Q. Wang, H. W. Liu, X. Yin, X. X. Hu, L. Yuan and X. B. Zhang, *Chem. Commun.*, 2019, **55**, 1758–1761; (*b*) W. W. An, L. S. Ryan, A. G. Reeves, K. J. Bruemmer, L. Mouhaffel, J. L. Gerberich, A. Winters, R. P. Mason and A. R. Lippert, *Angew. Chem., Int. Ed.*, 2019, **58**, 1361–1365; (*c*) C. Y. Liu, Y. W. Wang, C. C. Tang, F. Liu, Z. M. Ma, Q. Zhao, Z. P. Wang, B. C. Zhu and X. L. Zhang, *J. Mater. Chem. B*, 2017, **5**, 3557–3564; (*d*) Z. P. Liu and Q. Sun, *Spectrochim. Acta, Part A*, 2020, **241**, 118680; (*e*) S. H. Yuan, F. Y. Wang, G. C. Yang, C. F. Lu, J. Q. Nie, Z. X. Chen, J. Ren, Y. Qiu, Q. Sun, C. C. Zhao and W. H. Zhu, *Anal. Chem.*, 2018, **90**, 3914–3919; (*f*) K. Kawai, N. Ieda, K. Aizawa, T. Suzuki, N. Miyata and H. Nakagawa, *J. Am. Chem. Soc.*, 2013, **135**, 12690–12696; (*g*) M. W. Yang, J. L. Fan, W. Sun, J. J. Du, S. Long, K. Shao and X. J. Peng, *Chem. Commun.*, 2019, **55**, 8583–8586.
13 (*a*) M. G. Ren, B. B. Deng, K. Zhou, J. Y. Wang, X. Q. Kong and W. Y. Lin, *J. Mater. Chem. B*, 2017, **5**, 1954–1961; (*b*) K. Sunwoo, K. N. Bobba, J. Y. Lim, T. Park, A. Podder, J. S. Heo, S. G. Lee, S. Bhuniya and J. S. Kim, *Chem. Commun.*, 2017, **53**, 1723–1726; (*c*) F. Ali, S. Sreedharan, A. H. Ashoka, H. K. Saeed, C. G. W. Smythe, J. A. Thomas and A. Das, *Anal. Chem.*, 2017, **89**, 12087–12093.
14 (*a*) J. Y. Chen, S. Y. Chen, X. R. Zhao, L. V. Kuznetsova, S. S. Wong and I. Ojima, *J. Am. Chem. Soc.*, 2008, **130**, 16778–16875; (*b*) S. Maiti, N. Park, J. H. Han, H. M. Jeon, J. H. Lee, S. Bhuniya, C. Kang and J. S. Kim, *J. Am. Chem. Soc.*, 2013, **135**, 4567–4572.
15 (*a*) P. Liu, X. T. Jing, F. B. Yu, C. J. Lv and L. X. Chen, *Analyst*, 2015, **140**, 4576–4583; (*b*) K. B. Zheng, W. Y. Lin, D. Cheng, H. Chen, Y. Liu and K. Y. Liu, *Chem. Commun.*, 2015, **51**, 5754–5757; (*c*) C. Wei, X. F. Wang, X. Y. Li, X. Jia, X. Y. Hao, J. Y. Zhang, P. Z. Zhang and X. L. Li, *Spectrochim. Acta, Part A*, 2020, **227**, 117765.
16 M. G. Ren, Q. Y. Xu, S. J. Wang, L. Liu and F. G. Kong, *Chem. Commun.*, 2020, **56**, 13351–13354.
17 Y. Fang, W. Chen, W. Shi, H. Y. Li, M. Xian and H. M. Ma, *Chem. Commun.*, 2017, **53**, 8759–8762.

 This journal is © The Royal Society of Chemistry 2021